Proceedings of the
Annual Stability Conference
Structural Stability Research Council
Atlanta, Georgia, April 21-24, 2026

Behavior of a modular steel floor system subjected to gravity loading

Abdelrhman A. Ramadan[1], Rajshri Chidambaram Muthu Kumar[2],
Matthew R. Eatherton[3], Benjamin W. Schafer[4]

Abstract

A modular steel floor system referred to as FastFloor allows offsite fabrication and does not require concrete fill, which is expected to result in substantially faster erection time compared to conventional systems. The FastFloor module consists of a flat steel plate welded to the top of two steel beams. While the elimination of concrete from the floor system reduces construction time, and simplicity of the module form reduces labor, buckling of the untopped floor plate may occur when subject to extreme loading and therefore needs to be understood. This paper presents the results of a four-point bending test on a FastFloor module. The 5 ft wide x 40 ft span specimen was subjected to vertical loading at third points while vertical and horizontal displacements were measured and the buckling behavior of the steel floor plate was observed. The overall behavior of the specimen as subjected to vertical loading is discussed. Then, the buckling behavior of the plate is examined including amplitude and wavelength of the buckling waves. The effectiveness of the floor plate to resist compression stresses is investigated in terms of an effective width. Strain gage measurements of plate longitudinal strains are examined and compared to analytical predictions for effective width.

1. Introduction

The use of modular floor systems and the elimination of concrete fill are two ways to significantly increase speed of structural steel building erection. As such, the FastFloor system was specifically developed to increase construction speed. A FastFloor module consists of a steel plate welded to the top flanges of two steel beams where typical configurations may have spans up to 40 ft with 5 ft beam spacing. Each module is prefabricated in the shop, installed onsite, and connected to adjacent modules with field-installed fasteners such as bolts. Some configurations may include filler plates between modules and the FastFloor system can be used as either a floor or a roof system. A research project is being conducted to develop design procedures and define design constraints on the system to satisfy all applicable strength and serviceability requirements

[1] Graduate Research Assistant, Virginia Polytechnic Institute and State University, <abdelrhman@vt.edu>
[2] Graduate Research Assistant, Johns Hopkins University, <rchidam3@jhu.edu>
[3] Montague-Betts Professor of Structural Steel Design, Civil and Environmental Engineering, Virginia Polytechnic Institute and State University, <meather@vt.edu>
[4] Willard and Lillian Hackerman Professor of Civil and Systems Engineering, Johns Hopkins University, <schafer@jhu.edu>

including floor vibrations, acoustics, fire protection, and more. This paper focuses on strength for resisting gravity loads.

To understand the flexural behavior of modular steel floors systems such as the FastFloor system when subjected to gravity loading, it is necessary to understand and be able to predict buckling of the steel floor plates. In these types of systems, the floor plate directly participates in resisting flexural demands, and therefore contributes to the overall strength and stiffness of the structural module. However, because the plate is typically slender, its ability to carry compressive stresses and thus contribute to flexural capacity may be limited by buckling.

Buckling of the floor plate can affect several aspects of module behavior including the module flexural strength, whether the plate provides sufficient lateral bracing to the beams, and the demands on the plate to beam welds. To evaluate these effects, the buckling behavior of the plate needs to be examined in terms of buckling shape, amplitude, and wavelength. An effective width approach provides a useful framework for quantifying the contribution of the buckled plate to the overall flexural strength of the module. This information is essential for understanding both the structural role of the plate and the behavior of the welded connection, and for establishing reliable design assumptions for modular steel floor systems such as FastFloor.

To address these needs, a full-scale test is conducted on a FastFloor module subjected to gravity loading. The test configuration, instrumentation, and loading protocol are presented, and the global and local responses of the specimen are examined. Particular emphasis is placed on the buckling behavior of the steel plate, the resulting deformation modes, and the contribution of the plate to the overall flexural strength of the system. Strain measurements are used to evaluate the effective width of the plate after buckling. While additional testing is planned as part of the broader FastFloor research program, the results presented herein provide important insight into the structural behavior, and design considerations of modular steel floor systems under gravity loading.

2. Testing Program

2.1 Description of the FastFloor Test Specimen

The tested FastFloor specimen was selected to be representative of the configuration with a 5 ft wide module that would have filler plates on either side (filler plates not included in this test). As shown in Figure 1, the spacing between the module beams is 5 ft on center, and the span between the supporting girders is 40 ft on center. The module beams are W24×68, and the steel floor plate has a thickness of 3/8 in. The steel plate is welded to the module beams using staggered fillet welds, as shown in Figure 1. The connection between the module beams and the supports is a seated connection consisting of four 3/4-in bolts at each end of the beams as shown in Figure 2a. For stability during shipping and to aid in floor vibrations, steel angles, referred to herein as angle blocking, were installed between beam bottom flanges. For this specimen, angle blocking was L4×4×1/4, welded to the bottom flanges of the beams at L/3 and 2L/3, where L is the beam span length. In addition, two angle stiffeners, L4×4×1/4, were welded to the underside of the steel plate at the same locations. This specimen was originally constructed for a vibration testing program which included K-bracing. For this test, the K-bracing was cut as shown in Figure 2b. For the

previous vibration test, the plate extended beyond the beam on one side, but was cut 3 in. outside the beam flange for this test.

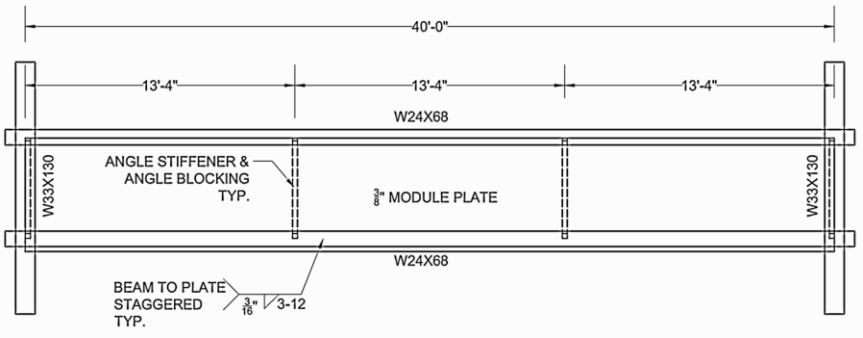

Figure 1: FastFloor specimen dimensions overview

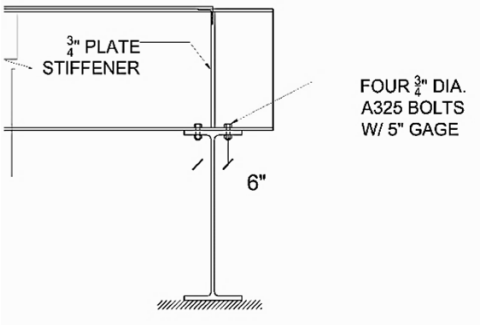

Figure 2: a) Seated connection at support;

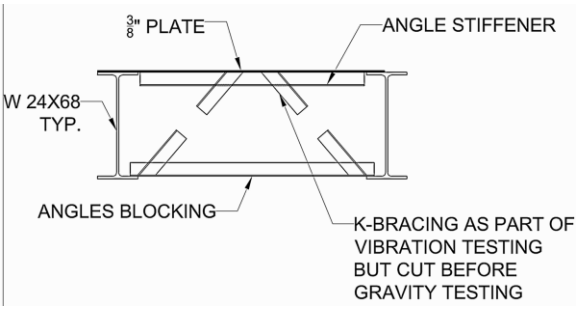

Figure 2: b) Specimen cross-section

2.2 Test Setup and Instrumentation

Figure 3 presents the test setup that consisted of a loading frame supporting a 500-kip-capacity hydraulic ram. The load was applied at the midspan of a spreader beam, which transferred the load to two loading beams located at third points in the beam span. A roller support was used at one end of the spreader beam, while the other end had a pin support. Each loading beam rested on 1 in. thick shim plates at the beam locations. The shim plates elevated the loading beams to prevent contact with the specimen steel plate, ensuring that the applied load was transferred directly to the specimen beams while allowing plate buckling. High-tension clamps were used to keep the loading beams in place on the specimen. The supporting girders at each end of the specimen were supported directly on the strong floor.

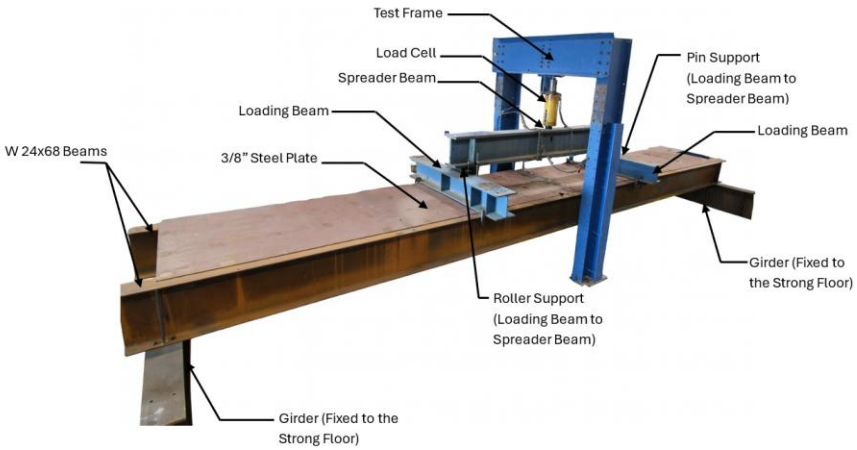

Figure 3: Test setup

Thirteen string potentiometers were attached to the specimen to measure vertical and horizontal displacements as shown in Figure 4. For vertical displacement measurements, three string potentiometers were attached to the bottom flange of each beam and three string potentiometers were attached to the underside of the steel plate. For horizontal displacement measurements, two string potentiometers were attached to the top and bottom flanges of both the east and west beams. Fifty strain gauges were attached to the specimen, divided into three strain-gauged sections. Section 1, shown in Figure 5, is located at midspan, where strain gauges are installed across the full cross section, including the beams and both the top and bottom surfaces of the steel plate. Strain-gauged Sections 2 and 3, shown in Figure 6, were located within the shear spans and strain gauges were attached only to the top and bottom surfaces of the steel plate.

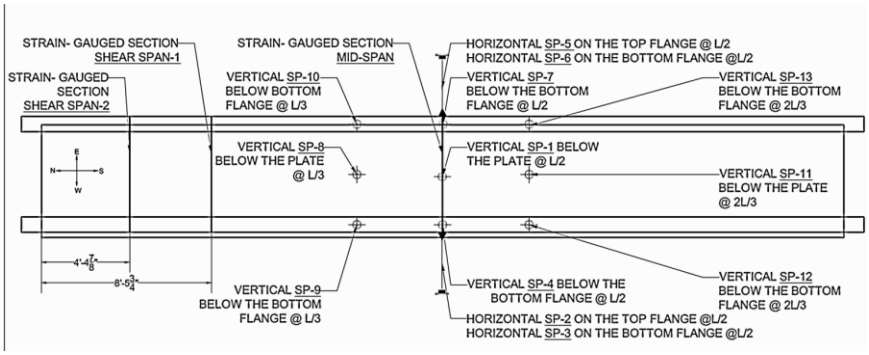

Figure 4: Instrumentation plan

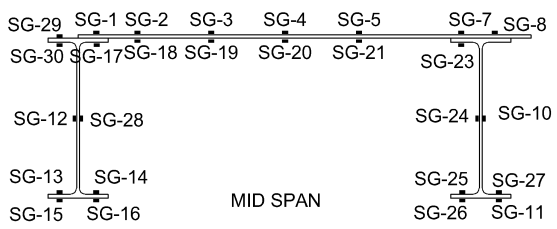

Figure 5: Section 1 strain gauges

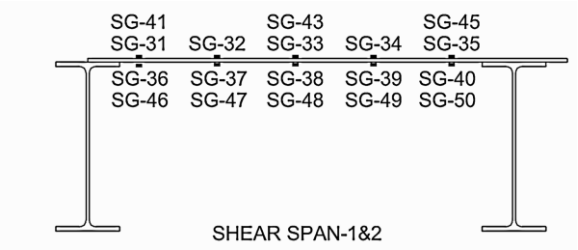

Figure 6: Sections 2&3 strain gauges

The load, measured using a load cell, was assumed to be applied evenly at four points, the third points of each beam. A displacement-controlled loading protocol was used with a target rate of 0.2 in/min. The control displacement was defined as the average displacement measured by the vertical string potentiometers SP-4 and SP-7, located at the midspan of the two beams.

3. Experimental Results

3.1 Global Load-Displacement Behavior

Figure 7 shows a plot of the total load measured by the load cell versus average displacement, calculated as the mean of the vertical displacements from SP-4 and SP-7 at the midspan of the two beams. The vertical axis on the righthand side of the plot shows the equivalent area load as the total load divided by the nominal area of the specimen (5 ft x 40 ft). The specimen initially exhibited elastic behavior, followed by reduced stiffness as inelasticity occurred. The response continued until a peak load of 335 kips was reached at an average displacement of 7.6 in, at which point one bolt at the seated connection between the beam and the girder at the north end of the specimen fractured. This fracture resulted in a sudden drop in load. As loading continued, the load

again reached 335 kips at an average displacement of 8.0 in, at which time a second bolt fractured at the same seated connection at the north end of the specimen. With further loading, the strength of the specimen was maintained until an average displacement of 8.7 in, when two bolts at the seated connection between the beam and the girder at the south end of the specimen fractured simultaneously. Following these bolt failures, excessive displacement at the loading points led to the test being stopped for safety concerns. For these reasons, the test was terminated and the specimen was unloaded.

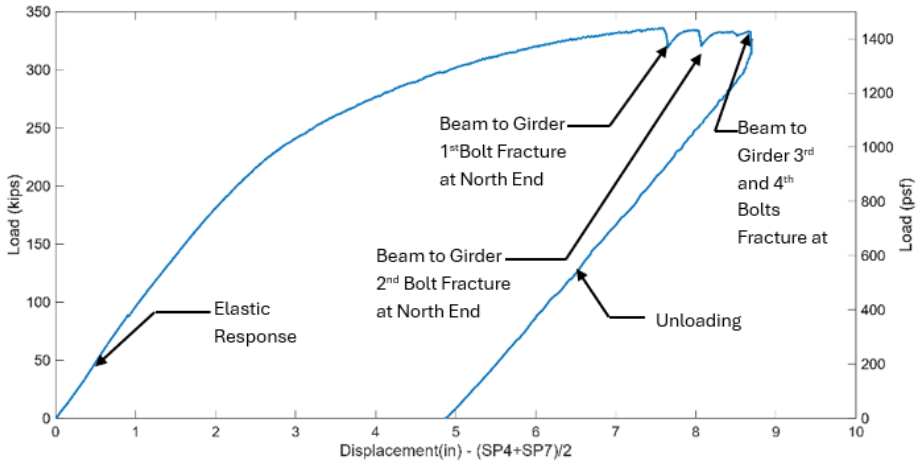

Figure 7: Load vs Average Displacement

3.2 Deformation Modes

Several deformation modes were observed as shown in Figure 8. The specimen midspan translated approximately 1.5 in. on average toward the east, which may be attributed to asymmetry of the steel plate. The plate stopped on the centerline of the east beam, but extended 3 in. past the flange tip of the west beam. This asymmetry results in unequal stiffness between the two beams, which may have contributed to the observed global translation. Second, the beams moved toward each other at midspan with the distance between beams shortening by 1 in. by the end of the test.

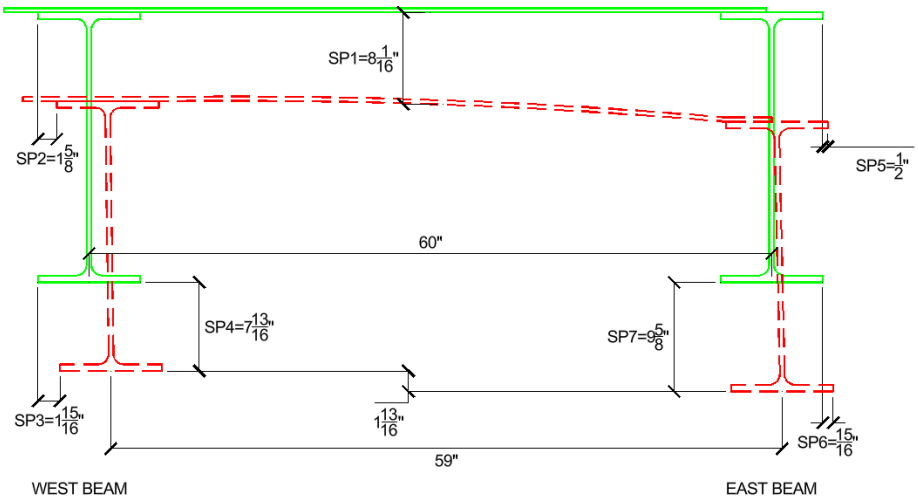

Figure 8: Specimen deformed shape

Twisting of the beams was also observed, as shown in Figure 8, where the beams twisted counterclockwise when looking north. This twisting may be influenced by imperfections in the beam cross-sectional geometry. Measurements of the as-built cross-section were recorded (Ramadan 2027).

Despite these deformations, no weld failure was observed during the test. Post-test inspection confirmed that all weld lines remained intact and maintained full contact between the steel plate and the beams.

3.3 Buckling Behavior of the Specimen

Another important observation from the test is the buckling behavior of the steel plate. Figure 9 shows the buckling shape of the plate within the constant moment region between the two loading beams.

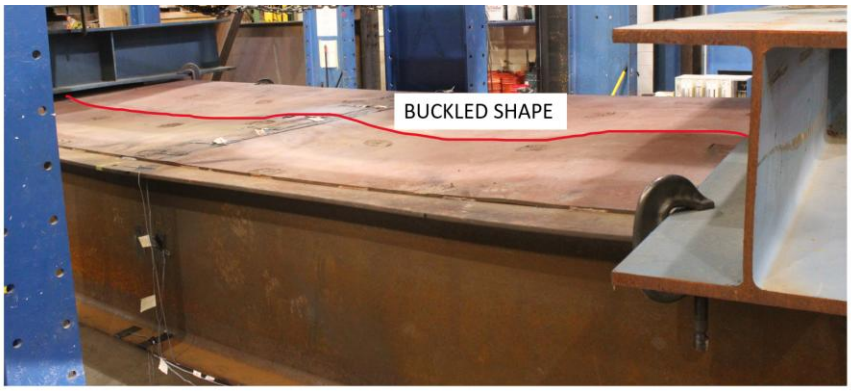

Figure 9: Buckling shape of the plate

Measurements were taken along the full span of the specimen, as shown in Figure 11, and included approximately six full waves across the full 40 ft span and 3 waves across the constant moment region that is 15 ft. The measured half-wavelength in the constant moment region is therefore approximately 2.5 ft.

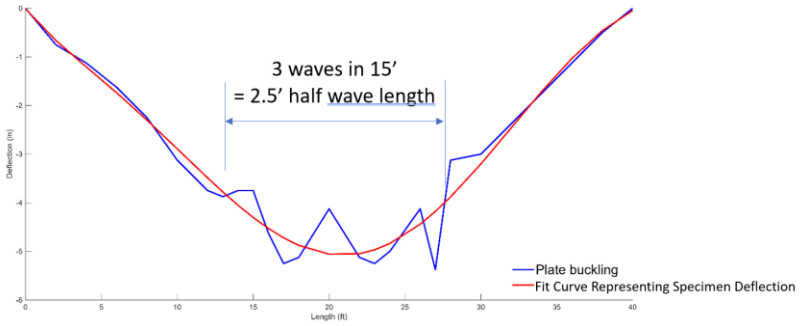

Figure 10: Measured plate buckling waves

Using the classical critical buckling stress formulation for a plate shown in Eq.1, (Bryan 1891) the buckling coefficient, k, shown in Eq.2 is estimated by substituting $m = 6$, corresponding to the observed number of buckling waves, and the plate aspect ratio, α. This calculation results in a buckling coefficient of $k = 4.3$, which is close to the theoretical value of $k = 4$ for a simply supported plate. This agreement suggests that the welded connection between the steel plate and the supporting beams provided boundary conditions that are consistent with simple support behavior for the plate under axial compression.

$$F_{cr} = k\pi^2 \frac{E}{12(1-\nu^2)} \left(\frac{t}{b}\right)^2 \quad (1)$$

$$k = \left(\frac{m}{\alpha} + \frac{\alpha}{m}\right)^2 \quad (2)$$

As discussed in the previously identified deformation modes, the out-of-plane sway of both specimen beams is associated with the overall buckling behavior of the specimen. The specimen can be idealized as a slender member undergoing out-of-plane buckling due to axial compressive forces induced by flexural action. Although the specimen was subjected only to gravity loading during the test, the corresponding axial compressive force that led to out-of-plane buckling can still be estimated.

To predict the critical axial force associated with this buckling mode, the Southwell method was used (Southwell 1932). Horizontal displacement data measured by the string potentiometers attached to the two beams were used to construct a Southwell plot, as shown in Figure 11. For this example, the data from the beginning of the test, when the specimen is elastic was used, specifically the data from string potentiometer SP5 which was horizontal displacement of the East beam top flange at midspan. From this plot, the critical buckling load was obtained from the slope of the linear relationship which showed that the elastic buckling load is equal to 326 kip. This plot and value of the buckling load is representative of all Southwell plots examined that were created using different horizontal string potentiometers.
It should be noted that the Southwell method is valid only prior to the onset of yielding, as it assumes that both the buckling curvature and the load–deflection response are governed by linear elastic behavior. For this reason, only data collected before yielding initiates were used in the construction of the Southwell plots.

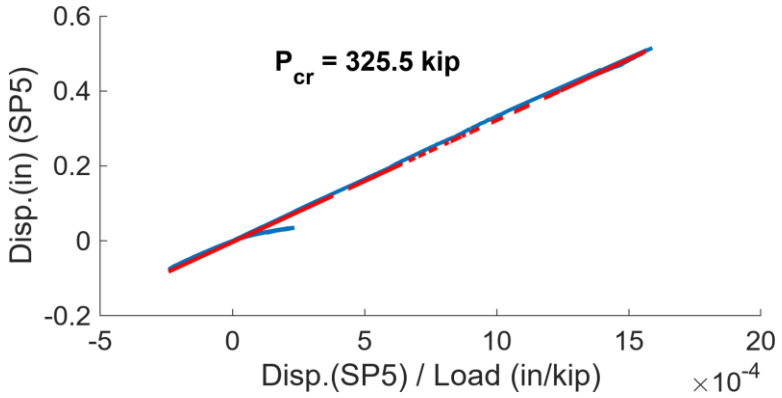

Figure 11: Southwell plot for the east beam top flange horizontal displacement

Two simplified empirical plate strength models were used to predict the in-plane compressive strength of a plate with the long sides intermittently supported as described by (Kumar et al. 2024). The simplified models are referred to herein as the limit state model and interacted model. These models can be used to predict the FastFloor plate strength with the approximation that both sides are assumed to be intermittently supported by welds at a uniform spacing.

The limit state model calculates the plate strength, P_{nLS} as the minimum of plate strength under global column buckling P_s and plate strength from Winter's equation P_w (Winter 1947). The spacing between welds, s= 12 in., was used in the calculation. The equations for this method are summarized in Eq.3 through Eq.5. The plate strength using the limit state model P_{nLS} is found to be 325 kip. This value will be compared to the force associated with measured strains in a later section.

$$P_{nLS} = \min(P_s, P_w) \tag{3}$$

where, P_s is the strength of the plate assuming global "column" buckling between fasteners, i.e

$$P_s = \begin{cases} 0.658^{\lambda_s^2} P_y & \lambda_s \leq 1.5 \\ \dfrac{0.877}{\lambda_s^2} P_y & \lambda_s > 1.5 \end{cases} \tag{4}$$

where, $\lambda_s = \sqrt{\frac{P_y}{P_{crs}}}$, $P_y = btF_y$, and $P_{crs} = \frac{\pi^2 EI}{s^2} = \frac{\pi^2 Ebt^3}{12s^2}$.
Further, P_w is the strength of the plate assuming Winter's effective width is valid, i.e.

$$P_w = \begin{cases} P_y & \lambda_w \leq 0.673 \\ P_y(1 - 0.22/\lambda_w)/\lambda_w & \lambda_w > 0.673 \end{cases} \tag{5}$$

where, $\lambda_w = \sqrt{\frac{P_y}{P_{crw}}}$, $P_y = btF_y$, and $P_{crw} = btf_{crw} = btk\frac{\pi^2 E}{12(1-\nu^2)}\left(\frac{t}{b}\right)^2$.

The interacted model follows (Peköz's 1986) unified approach in concept. The plate strength, P_{nI} is found using the Winter curve expression, except that the yield strength is limited to the column stress P_s which is found using the AISC column curve. The equations for this method are summarized in Eq.6. The plate strength using the interacted model P_{nI} is found to be 186 kips. This value will be compared to the force associated with measured strains in a later section.

$$P_{nI} = \begin{cases} P_s & \lambda_{ws} \leq 0.673 \\ P_s(1 - 0.22/\lambda_{ws})/\lambda_{ws} & \lambda_{ws} > 0.673 \end{cases} \tag{6}$$

where, $\lambda_{ws} = \sqrt{\frac{P_s}{P_{crw}}}$, P_s and P_{crw} as previously defined.

3.4 Plate effective Width

The strain gauges installed at the midspan cross section provided strain data that were used to evaluate the effective width of the steel plate. This evaluation is essential for determining the flexural capacity of the FastFloor module. Different methods were employed to estimate the plate effective width, and the results were compared with code-based predictions.

Figure 12 shows the measured strain distribution at the midspan cross section at the peak displacement of the specimen. A plane fitted to the measured strains across the full cross section,

including the beams and the steel plate. This fitted strain plane intersects the beam cross section at a location where the strain is zero, which can be interpreted as the neutral axis of the section.

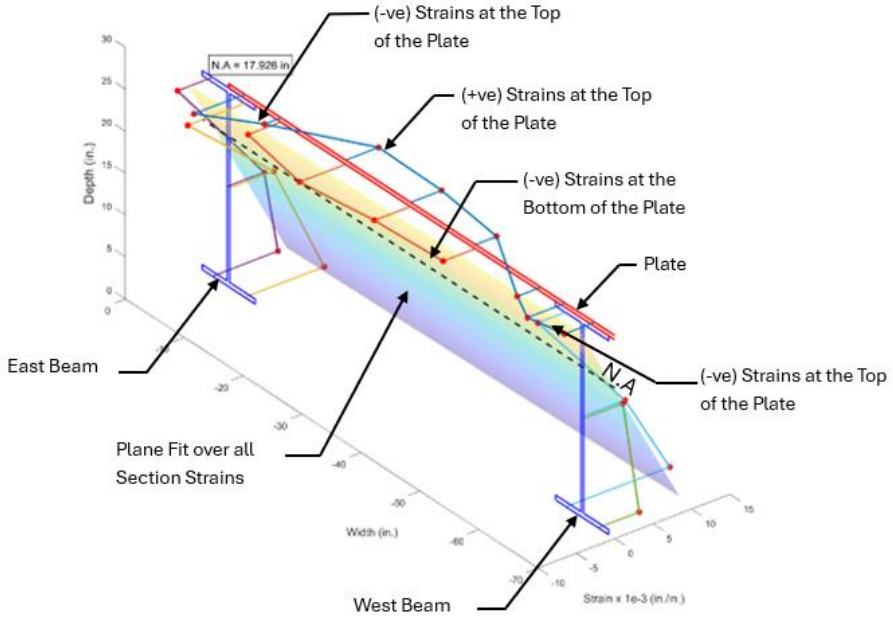

Figure 12: Plane fit to the measured mid-span cross section strains at the time of peak displacement

Because the strains were well past yield, the location of zero strain was assumed to be the plastic neutral axis. For a plastic stress distribution, the effective width can be determined by assuming every fiber of the section was yielding and enforcing force equilibrium such that the total compressive force equals the total tensile force. Using this approach, the calculated plate effective width for each beam is $b_{eff} = 11.5$ in. This implies that less than 40% of the plate is effective in contributing to flexural strength.

In the second method, the plate effective width was estimated using an equivalent stress block approach. In this method, only the strain measurements on the top and bottom surfaces of the steel plate were considered, excluding the beams. The average of the top and bottom plate strains was taken to represent the axial strain in the plate at that point. By multiplying this axial strain by the modulus of elasticity, but not letting the value exceed the yield stress of the steel, F_y=56.7 ksi, the corresponding axial stress distribution across the plate width was obtained as shown in Figure 13. The area under the resulting stress distribution curve was then equated to an equivalent uniform stress block, whose width was defined as the plate effective width. This method resulted in an effective width for each beam of $b_{eff} = 29$ in. This effective width is associated with a total axial force in the plate equal to 1231 kips, and a moment strength for the entire specimen of 2154 kip-ft.

The plate axial force obtained from experimental strains, 1231 kips, is significantly larger than what was predicted using theoretical equations for plate buckling with simply supported boundary conditions. The limit state model, described in the previous section, resulted in a plate axial force equal to $P_{nLS} = 325\ kip$ while the interacted model predicted $P_{nI} = 186\ kip$. This difference is related to the effective width that the simplified models predict.

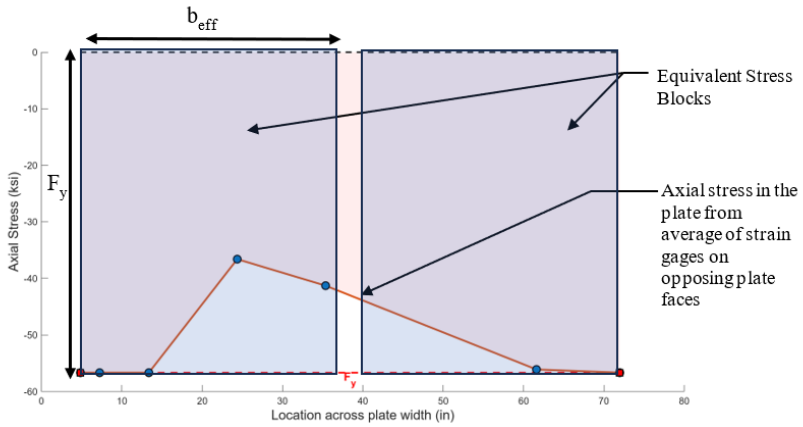

Figure 13: Area under the stress curve converted to an equivalent stress block.

The effective width can also be calculated based on theoretical models. Winter's effective width equation (Winter 1947) predicts the effective width of the plate using a reduction factor ρ that accounts for the local buckling in thin plates subjected to axial compression. Winter's effective width expression is shown in Eq.7 and Eq. 8. The effective width for each beam b_{eff} was found using the reduction factor multiplied with half the actual width of the plate $b = 60\ in$. The reduction factor was decided based on the slenderness of the plate λ shown in Eq. 9. The yield strength used is $F_y = 56.7\ ksi$, and the elastic critical stress F_{cr} was found using Eq. 1 which was developed by (Bryan 1891). For the FastFloor specimen considered in this study, the plate has a thickness $t = 0.375$ in., Young's modulus $E = 29000$ ksi, and Poisson's ratio $\nu = 0.3$. The buckling stress coefficient, $k = 4$ was used since the plate was under simply supported conditions. Using these factors, the effective width for each beam was found as $b_{eff} = 7.6$ in.

$$b_{eff} = \rho b/2 \tag{7}$$

$$\rho = \begin{cases} 1 & \lambda \leq 0.673 \\ (1 - 0.22/\lambda)/\lambda & \lambda > 0.673 \end{cases} \tag{8}$$

$$\lambda = \sqrt{F_y/F_{cr}} \tag{9}$$

The effective plate width that was first estimated using Winter's effective width formulation, which was based on elastic local buckling behavior and represented the maximum plate portion capable of reaching the yield stress provided an upper-bound estimate of the plate contribution and was used to form an initial plastic section modulus including the plate. However, Winter's effective width formulation does not account for the ability of the plate to sustain large inelastic strains required for plastic hinge development. To obtain a strain-compatible estimate of plate participation, a refined approach based on strain-based slenderness limits was subsequently adopted. A target strain demand of at least $3\varepsilon_y$ was assumed to represent the strain levels associated with plastic moment development. Consistent with the Continuous Strength Method (CSM) (Gardner, Yun, and Walport 2023) framework and equivalent to the non-dimensional plastic slenderness limits for stiffened elements in (AISC 360), this strain requirement corresponds to a limiting plate slenderness of λ_{plate} that is shown in Eq. 10

$$\lambda_{plate} = \sqrt{\frac{F_y}{F_{cr}}} = 0.46 = \sqrt{\frac{F_y}{k\frac{\pi^2 E}{12(1-\nu^2)}\left(\frac{t}{b_{eff}}\right)^2}} \quad (10)$$

At this limiting slenderness, the effective plate width was back-calculated using the elastic plate buckling expression shown in Eq. 10, resulting in a reduced effective width suitable for sustaining plastic strain demands. This strain-compatible effective width was then used to recompute the plastic section modulus and corresponding plastic moment capacity including the plate contribution. Using this method, the effective plate width for each beam is calculated as $b_{eff} =$ 5.3 in., resulting in a moment strength of 1845 kip-ft.

Using the (AISC 360) composite section provisions chapter I section 1a, which resulted in an effective plate width for each beam of $b_{eff} = 30$ in, the resulting moment strength is 2156 kip-ft. This indicates that the effective width of the FastFloor module can be best described by the (AISC 360) effective width calculation.

To evaluate the efficacy of the different plate effective width predictions, Figure 14 shows the moment strength of the specimen compared with the analytical predictions. The experimental moment strength was obtained as the applied load multiplied by the length of the shear span in this four-point bending test. The experimentally observed peak moment strength of the specimen was found to be 2240 kip-ft. The predicted moment strengths based on theoretical models were found to be much smaller than the peak moment observed experimentally. The comparison shows that the peak moment is best captured by either the effective width calculated from an equivalent stress block method, $b_{eff} = 29$ in., or using the full width of the plate, $b_{eff} = 30$ in.

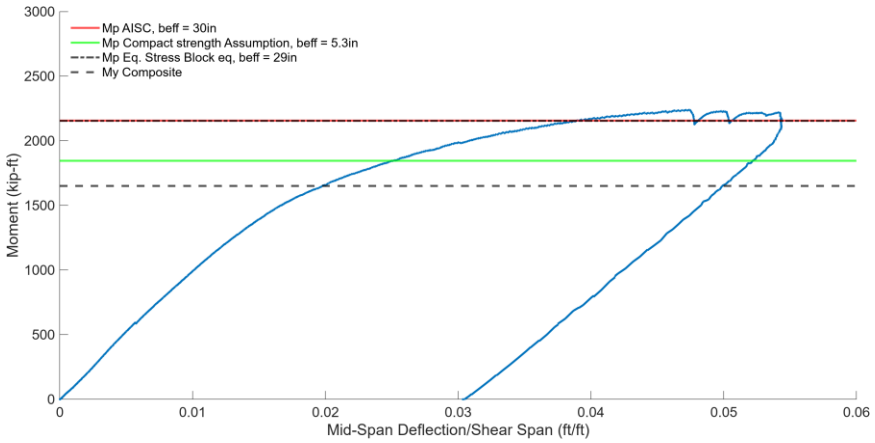

Figure 14: Comparison of the plastic moment capacity using various plate width assumptions

4. Conclusions

A gravity load test was conducted on a modular steel floor specimen known as FastFloor. The test demonstrated that the system was able to develop significant flexural strength while experiencing multiple deformation modes. The steel plate welded to the beams contributed meaningfully to the overall stiffness and strength of the module, even after plate buckling plate occurred. The onset of strength degradation in the test was governed by fracture of bolts at the seated beam-to-girder

connections rather than by failure of the steel plate or welded connections. This indicates that connection behavior plays a critical role in the ultimate response of the system under gravity loading.

Buckling of the steel plate developed in a stable and repeatable pattern within the constant moment region. The observed buckling wavelength and shape are consistent with classical plate behavior and indicated that the welded connection between the plate and the beams provided boundary conditions similar to simple support. Plate buckling did not lead to weld fracture as all welds remained intact throughout the test. Strain measurements at midspan show that all of the plate width contributed to specimen moment strength despite plate buckling. Methods for predicting the plate effective width were presented and evaluated.

Overall, the results demonstrated that the untopped steel plate in the modular floor system can sustain significant post-buckling stresses and contribute to flexural capacity without compromising weld integrity. These findings support the viability of the modular steel floor system under gravity loading and provide a basis for rational design assumptions regarding plate buckling, and effective width.

Acknowledgements
This work was sponsored by the Charles Pankow Foundation, American Institute of Steel Construction (AISC), MKA Foundation, Nucor Corporation, Schuff Steel, Herrick Steel, Cives Steel, Zekelman Industries (Atlas Tube/Shuriken), Owen Steel, Metals Fabrication and SDI Steel Dynamics. In-kind support was provided by Cerami, Sherwin-Williams, Cooper Steel, Clark Construction, Hensel Phelps, Tate and Pliteq. Any opinions, findings, and conclusions or recommendations expressed in this material are those of the authors and do not necessarily reflect the views of the sponsors and supporters.

References

Bryan, G. H. (1891). On the stability of a plane plate under thrusts in its own plane. *Proceedings of the London Mathematical Society,* 22, 54–67.

Southwell, R. V. (1932). On the analysis of experimental observations in problems of elastic stability. *Proceedings of the Royal Society of London*, Series A, 135(828), 601–616.

Kumar, R. C. M., Torabian, S., and Schafer, B. W. (2024). "Effect of intermittent edge support on in-plane plate compressive strength." *Proceedings of the Annual Stability Conference, Structural Stability Research Council*, San Antonio, Texas, March 19–22.

Peköz, T. (1986). "Development of a Unified Approach to the Design of Cold-Formed Steel Members." *Report to the American Iron and Steel Institute*, Washington, D.C.

American Institute of Steel Construction. (2016). *Specification for Structural Steel Buildings (ANSI/AISC 360-16).* Chicago, IL.

Gardner, L., Yun, X., & Walport, F. (2023). "The Continuous Strength Method — Review and outlook". *Engineering Structures*, 275, Article 114924

Winter, G. (1947). "Strength of thin steel compression flanges." *Transactions of the American Society of Civil Engineers*, 112, 527–554.

Ramadan, A. (2027). Behavior of a modular steel floor system. *Doctoral dissertation*, Virginia Polytechnic Institute and State University, Blacksburg, Virginia.